Aeroelastic Modeling of Rotor Blades with Spanwise Variable Elastic Axis Offset - Classic Issues Revisited and New Formulations

by

Richard L. Bielawa
Senior Research Scientist
United Technologies Research Center
East Hartford, CT
06108

Abstract

In response to a systematic methodology assessment program directed to the aeroelastic stability of hingeless helicopter rotor blades, improved basic aeroelastic reformulations and new formulations relating to structural sweep have been achieved. Correlational results are presented showing the substantially improved performance of the G400 aeroelastic analysis incorporating these new formulations. The formulations pertain partly to sundry new solutions to classic problem areas, relating to dynamic inflow with vortex-ring state operation and basic blade kinematics, but mostly to improved physical modeling of elastic axis offset (structural sweep) in the presence of nonlinear structural twist. Specific issues addressed are an alternate modeling of the ΔEI torsional excitation due to compound bending using a force integration approach, and the detailed kinematic representation of an elastically deflected point mass of a beam with both structural sweep and nonlinear twist.

Nomenclature

B	Tip loss factor
C_L, C_M	Rotor roll and pitch moment coefficients, respectively, (moment/$\rho\pi\Omega^2R^5$), ND
C_T	Rotor thrust coefficient ($T/\rho\pi\Omega^2R^4$), ND
EI_y, EI_z	Section bending stiffness in flatwise and edgewise directions, respectively, lb-in^2 or ND, ($\Delta EI = EI_z - EI_y$)
$\mathcal{F}$	Induced velocity function, ND
F_T	Tension cosine resolution function, ND
K	Induced velocity gradient factor, ND
p_{x_5}, p_{y_5}, p_{z_5}	Section shear load distributions in directions of "5" coordinate system, ND
q_{v_k}	Blade k'th edgewise modal response variable
q_{w_i}	Blade i'th flatwise modal response variable
q_{x_5}, q_{y_5}, q_{z_5}	Section moment load distributions about axes in the "5" coordinate system, ND
q_{θ_j}	Blade j'th torsion modal response variable
R	Rotor radius, ft.
r	Blade spanwise coordinate, measured from offset in x_5 direction, ND
S_{x_2}	Component of load distribution in radial (x_2) direction, ND
T	Tension at blade section, or rotor thrust, as appropriate, lbf.
$[TAS]$	Coordinate transformation matrix relating "5" and "6" coordinate systems, due to structural sweep, ND
u_e	Inward radial (x_5) foreshortening of blade element point due to combination of built-in sweep and elastic deformation, ND
v	inflow parameter
v_e, w_e	Elastic deflections in the edgewise and flatwise directions, respectively, ND
v_o	Uniform component of momentum induced velocity, ND
v_{l_c}, v_{l_s}	Cosine and sine components, respectively, of momentum induced velocity, ND
Δv, Δw	Deflection correction functions due to first order twist effects, ND
ΔV, ΔW	Deflection correction terms due to second order twist effects, ND
x_5, y_5, z_5	Components of position vector in the "5" system (rotating, coned and lagged), ND
$y_{5_{EA}}$, $z_{5_{EA}}$	Built-in offset distances of elastic axis from x_5 axis in inplane and out-of-plane directions, respectively, ND
$y_{10_{EA}}$, $z_{10_{EA}}$	Built-in offset distances of elastic axis from x_5 axis, in edgewise and flatwise directions, respectively, ND
β_B	Built-in blade precone, deg.
$\Delta\beta$	Built-in precone outboard of pitch bearing (negative droop), deg.
$\Gamma_{y_{\epsilon_j}}$, $\Gamma_{z_{\epsilon_j}}$	Nonlinear j'th torsion modal weighting functions for torsion excitation due to edgewise and flatwise force loadings, respectively, ND
$\tilde{\Gamma}_{y_{\epsilon_j}}$, $\tilde{\Gamma}_{z_{\epsilon_j}}$	Nonlinear j'th torsion modal weighting functions for torsion excitation due to flatwise and edgewise moment loadings, respectively, ND
γ_E γ_F	Inplane and out-of-plane slope projection angles, respectively, defining blade element orientation, rad.
γ_{v_k}	Deflection mode shape for the k'th edgewise normal mode, ND
γ_{w_i}	Deflection mode shape for the i'th flatwise normal mode, ND
γ_{ϵ_j}	Deflection mode shape for the j'th torsion normal mode, ND
θ	Total local blade pitch angle, radians
θ_e	Elastic torsion deflection angle, radians
θ_o	Collective pitch angle, deg.
Λ_{e_5}	Structural sweep angle projection onto x_5-y_5 plane, rad.
Λ_{f_5}	Structural sweep angle projection onto x_5-z_5 plane, rad.

Presented at the ITR Methodology Assessment Workshop at Ames Research Center, Moffett Field, California, June 1983.

$\lambda(r,\psi)$	Inflow ratio with spanwise and azimuthal variability, ND
$\hat{\lambda}$	Normalized rotor through flow parameter, ND
λ_{RAM}	Part of uniform inflow arising from rotor forward flight, ND
λ_o	Uniform component of variable inflow, ND
μ	Rotor advance ratio, ND
ρ	Air density, lb-sec^2/ft^4
σ	Alternately, rotor solidity, and real part of eigenvalue, ND
ψ	Blade azimuth angle, rad.
Ω	Rotor rotation speed, rpm.

Subscripts and Superscripts

$(\ )_e$	Due to elastic deformation
$(\ )_{EA}$	Defined at the elastic axis
$(\ ^*)$	Differentiation with respect to ψ
$(\ )'$	Differentiation with respect to (r/R)
$(\ \hat{}\ )$	Denotes evaluation at zero collective angle as applied to deflections

Introduction

For most production helicopter design applications, the principal role of contemporary comprehensive rotor aeroelastic analyses has been that of providing calculations of forced structural responses and, in particular, of blade dynamic stresses. The United Technologies Corporation family of G400 rotor aeroelastic analyses comprises such a comprehensive analysis technology and has undergone extensive development in the last ten years with this principal role as a prime objective. The present G400 technology has evolved from an analysis originally formulated for the unique aeroelastic characteristics of the composite bearingless rotor. That analysis represented an advancement in the state-of-the-art with regard to the modeling of rotors with time-variable, nonlinear structural twist and multiple structural redundancy, as described in Reference 1. The G400 technology which has evolved now includes a family of four actively used versions with a completely general range of applicability in rotor type (articulared, hingeless, teetered and gimballed) and vehicle application (helicopters, propellers and wind turbines). The mathematical modeling capabilities of the G400 analyses are summarized in Figure 1.

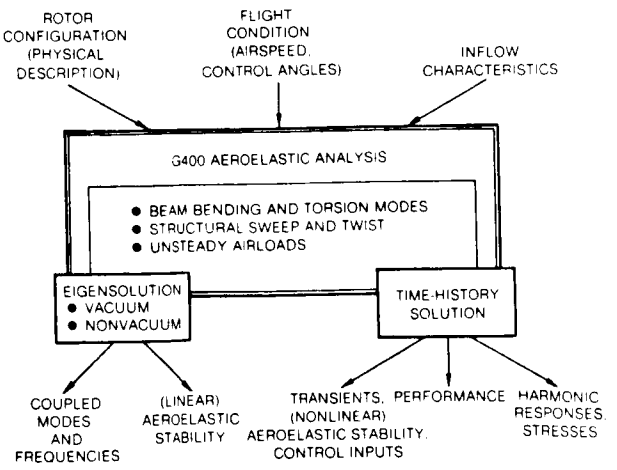

Fig. 1 - Basic capabilities of G400 Aeroelastic Analyses.

Of the two major solution types, eigensolution and time-history solution, the latter contains the most complete physical modeling of the blade aeroelasticity. This includes the dynamics, airloads, excitations and kinematic couplings with the full retention of all nonlinearities which have been identified as being potentially germaine to the aeroelastics. Thus, no nonlinearities have been deleted from the time-history solution for reasons of mathematical convenience. Prior to 1983, the major documentation of the G400 technology was available only in References 1 through 3. Since completion of the work reported herein, another major documentation source has become available (Reference 4).

Within the context of only forced response calculations, limited harmonic response correlation studies have been performed. These have been conducted principally under corporate and contractual funding; References 5 and 6 are the available documentations of this type of correlation study. Detailed aeroelastic stability correlation studies, however, had not been performed prior to the performance of the Integrated Technology Rotor/Flight Research Rotor (ITR/FRR) Methodology Assessment study (Reference 7). One reason for the lack of G400 stability correlation calculations is clearly the emphasis placed on forced response loads calculations by the principal users of the code. Another more logistical reason, however, is that over most of its development life the G400 analysis has been principally a time-history solution analysis. As a result, the eigensolution capability had not kept pace with the increased sophistication of this time-history solution capability. Consequently, accurate stability calculations have typically required the use of transient time-history calculations. Such calculations are generally both time and cost intensive and, hence, had been eschewed. Despite the cost disadvantage, however, time-history solutions present a distinct advantage in the calculation of transient stability, as is discussed in greater detail in a subsequent section.

Under contract NAS2-10864, the in-house helicopter version of G400 was exercised for stability correlation as part of this methodology assessment study. Initial results of this study were generally poor. The G400 stability predictions were deemed unacceptably inaccurate and a concerted corporate-sponsored methodology improvement project was initiated. The general results of this improvement project were completely successful. The stability predictive capability of G400 was definitely raised to an acceptably accurate level (giving good to excellent correlation results) while retaining a valid, mathematically consistent formulation. Over and above this immediate positive result, however, this methodology improvement study produced new formulations and revised existing ones; these formulations are of interest in their own right.

The nature of the detailed reformulations were of three main types: The first consisted of the detection and correction of outright errors in the programmed implementations of the existing derived equations. The second consisted of a sundry class of modifications wherein established aeroelastic methodology was extended from the generally accepted norm. And the third consisted of an improved representation of structural sweep. A discussion of the first type of reformulation is clearly inappropriate for publication and is omitted from further discussion. The second and third types of reformulation, however, constitute new knowledge and form the basis of this paper. The remainder of this paper is divided into three main sections: (1) a review of the pertinent G400/ITR correlation results, (2) a description of the sundry modifications arising from enhanced reformulations of existing theory, and (3) a description of the new formulations relating to structural sweep.

Review of Pertinent ITR Correlation Results

The ITR Methodology Assessment Study, as defined in Reference 7, concentrated on the aeroelastic stability characteristics of hingeless and/or bearingless rotors both in hub-fixed and hub-flexible configurations. Particular emphasis was placed on the stability of the already lightly damped blade edgewise (inplane) mode as affected by couplings with the blade flatwise (out-of-plane) and torsion modes, and with the flexible hub degrees-of-freedom. In all cases, the pertinent mode, whose stability characteristics were to be calculated, was characterized by relatively low reduced frequencies along the blade and for most conditions by an absence of stall. Hence, the stability phenomena could be assumed to be reasonably well-governed by conventional quasi-static airloads.

The original results from applying G400 to the experimental correlational data were generally poor for most of the configurations defined in the study. Of particular significance were the poor correlations achieved with the simplest configuration: that of an isolated hingeless model rotor with no twist or cyclic pitch (configuration IIA, as described in detail in Reference 8). Although the other configurations were equally, if not more, important to the ITR study as a whole, only this configuration will be addressed in this paper because it was the primary vehicle which led to the enhancements to be discussed herein.

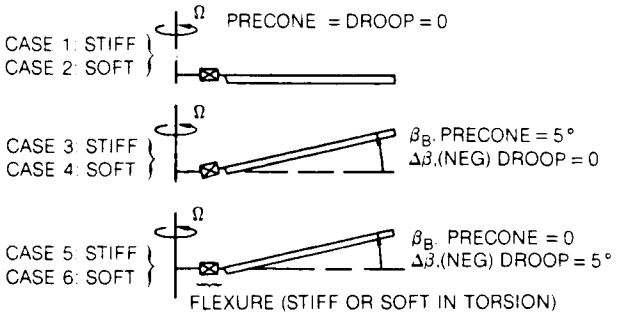

Fig. 2 Correlation cases for ITR configuration IIA, isolated hingeless rotor.

The configuration IIA rotor stability data consisted of 6 distinct cases involving simple parameter variations in precone, β_B, droop, (-)$\Delta\beta$, and torsional flexure stiffness, as shown in Figure 2. A measure of the torsional stiffness of the two flexures is afforded by the first torsional mode amplitudes near the blade root. For the stiff and soft flexures, the calculated torsion modal amplitudes (at the 3% spanwise location) were, respectively, .00013 and 0.12754. For each of these parameter variations, the damping constant, σ, was obtained as a function of blade collective angle, θ_0, as shown in Figures 3a thru 3f. These figures present the experimentally obtained values together with the initial (12/81) G400 calculations and the updated (5/83) ones. The improved correlation of the updated G400 results is apparent and is generally representative of all the results obtained by including the three types of reformulations. These figures will be referred to in the subsequent sections to illustrate the impact of the various specific reformulations.

(a) Case 1 - stiff flexure, $\beta_B = \Delta\beta = 0$.

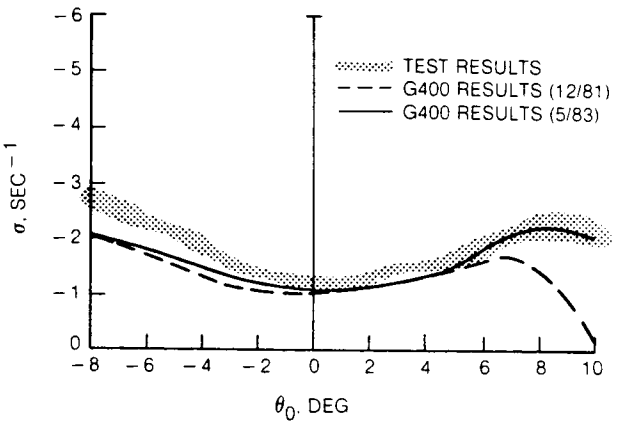

Fig. 3 - Comparison of experimental results with initial and revised G400 calculations-configuration IIA.

(b) Case 2 - soft flexure, $\beta_B = \Delta\beta = 0$.

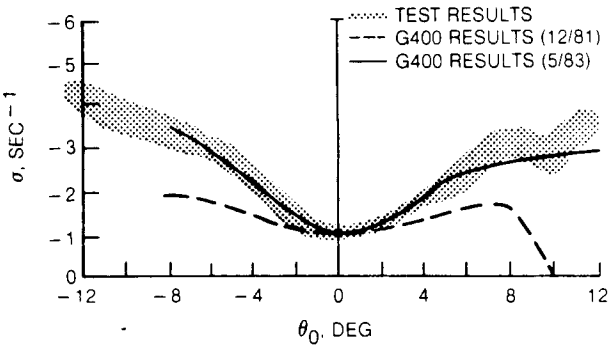

(c) Case 3 - stiff flexure, $\beta_B = 5^o$, $\Delta\beta = 0$.

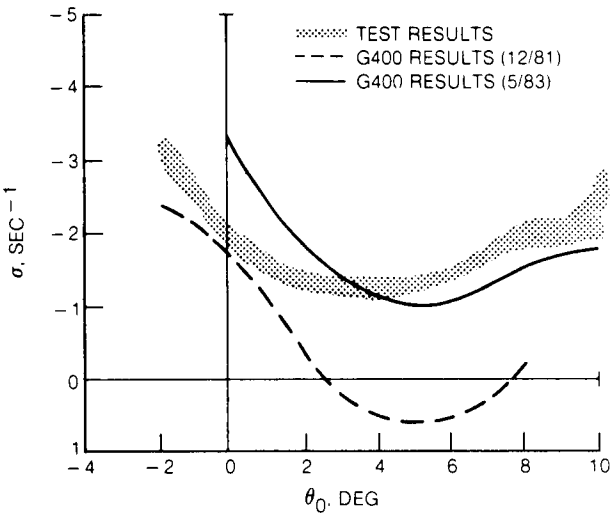

(d) Case 4 - soft flexure, $\beta_B = 5^o$, $\Delta\beta = 0$.

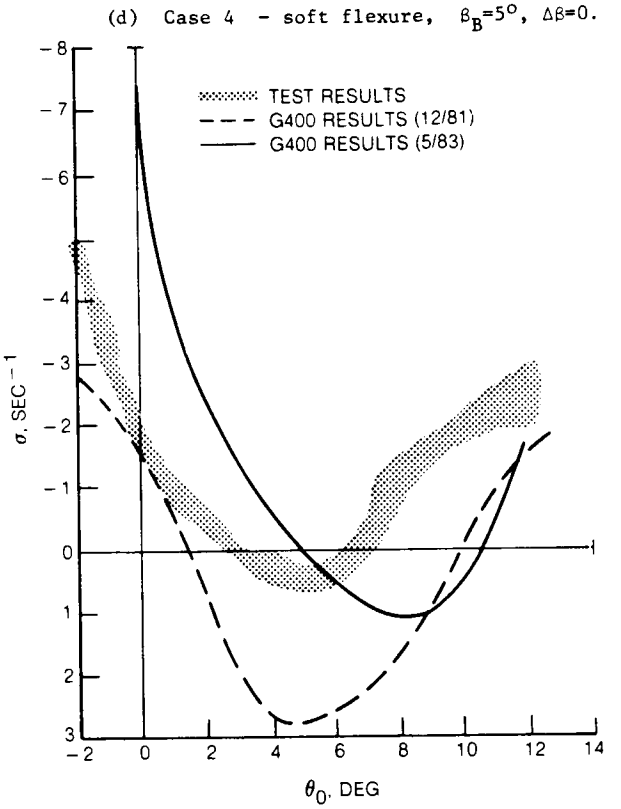

(e) Case 5 - stiff flexure, $\beta_B = 0$, $\Delta\beta = -5^o$.

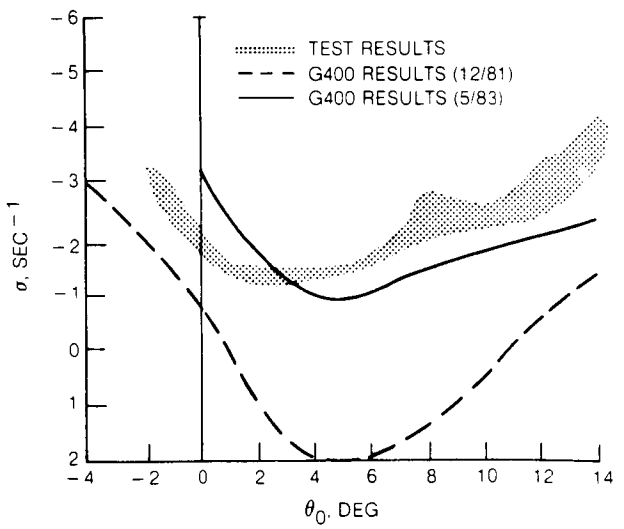

(f) Case 6 - soft flexure, $\beta_B = 0$, $\Delta\beta = -5^o$.

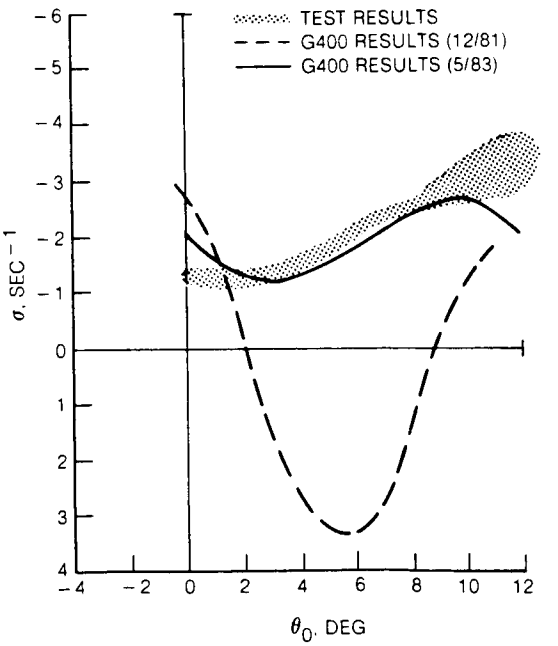

Fig. 3 continued - Comparison of experimental results with initial and revised G400 calculations-configuration IIA.

Sundry Reformulations Relating to Existing Theory

Air Mass Dynamics

Examination of Figures 3a and 3b shows an experimentally observable falloff of rotor stability at sufficiently high values of collective angle. The most obvious inaccuracy of the initial G400 calculations is the premature falling off of the damping constant with increasing collective angle. The physics governing this attenuation of damping is twofold: First, increases in collective will necessarily increase the blade loading and, thereby, the static out-of-plane blade bending. This increase in static bending will significantly impact on the effective pitch-edge coupling which, in large measure, defines the pitch-flap-lag stability. Secondly, increases in collective will also increase the penetration of the blade section angles-of-attack into the near stall, high drag rise coefficient regime of airfoil operation. As shown in Reference 8, this regime of rotor operation is generally destabilizing. The basic parameter common to and controlling each of these effects is the local blade section angle-of-attack. The angle-of-attack, however, is determined from both geometric and inflow contributions. From inspection of the initial G400 results it appeared that the section angle-of-attack vs. pitch angle relationship might be incorrect and such in fact was the case.

The G400 technology incorporates a representation of air mass dynamics which closely conforms to the established state-of-the art (e.g. Reference 9). The major departure of the G400 technology from that typified by Reference 9 is twofold. First, the technology employs a nonperturbational, totally nonlinear form of the momentum equations. Second, in order to accommodate the high thrust loadings at which a wind turbine is capable of operating, the G400 technology employs an empirical correction procedure for simulating operation in or near the vortex-ring state. These ideas are summarized in the following development. The total (nonperturbational) form of momentum variable inflow is assumed to be as follows:

$$\lambda(r,\psi) = \lambda_{RAM} - v_0 - r\left[(v_{1_C} + K v_0)\cos\psi + v_{1_S}\sin\psi\right] \tag{1}$$

where the Glauert factor, K, is approximated[10] by the following simple expression:

$$K = \frac{4}{3}\,\frac{(\mu/\lambda_0)}{1.2 + (\mu/\lambda_0)} \tag{2a}$$

, where:

$$\lambda_0 = \lambda_{RAM} - v_0 \tag{2b}$$

and where v_1, v_{1_C} and v_{1_S} are the uniform (zeroth harmonic), and first harmonic components of induced velocity, respectively. These components of induced velocity are governed by appropriate first order differential equations:

$$\overset{*}{v}_0 = \frac{3\pi}{4}\left[\frac{C_T}{2B^2} - \frac{v_0}{\mathcal{F}}\right] \tag{3}$$

$$\begin{Bmatrix} \overset{*}{v}_{1_C} \\ \overset{*}{v}_{1_S} \end{Bmatrix} = \frac{45\pi}{16}\left\{\frac{1}{B^3}\begin{bmatrix} -C_M \\ C_L \end{bmatrix} - v\begin{bmatrix} v_{1_C} \\ v_{1_S} \end{bmatrix}\right\} \tag{4}$$

where $\mathcal{F}$ is a newly-defined rotor induced velocity function whose independent variable is taken to be the normalized through-flow parameter defined as follows:

$$\hat{\lambda} = \mathrm{sgn}(\lambda_0 C_T)\sqrt{\mu^2+\lambda_0^2}\,\Big/\sqrt{|C_T|/2B^2} \tag{5}$$

and the usual inflow parameter, v, is defined as:

$$v = \frac{\mu^2 + \lambda_0(\lambda_0 - v_0)}{\sqrt{\mu^2+\lambda_0^2}} \tag{6}$$

For rotor operation well removed from the vortex ring state ($|\hat{\lambda}| \geq 1.4$) the rotor induced velocity function, $\mathcal{F}$, consists of two branches and is directly obtainable from standard momentum theory as given simply by $1/|\hat{\lambda}|$. For values of $|\hat{\lambda}|$ less than 1.4 and especially approaching zero, the momentum representation breaks down (and eventually goes singular). Alternate empirical correction curves which connect the two valid momentum branches for values of $\hat{\lambda}$ between -1.4 and +1.4 are suggested by material presented both by Gessow and Myers [11] and by Lissaman, as shown in Figure 4.

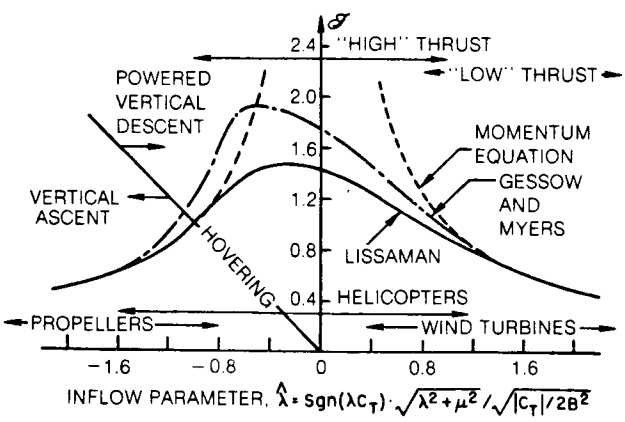

Fig. 4 Rotor induced velocity function.

Essentially the reformulations pertaining to air mass dynamics which were included in the updated G400 technology were to include the signum function factor in the definition for $\hat{\lambda}$, as given in Equation (5) (in order to accommodate negative values of inflow, λ), and to abandon the Lissaman data in favor of the Gessow and Myers data. For the configuration IIA correlation cases, these changes resulted in values of $\mathcal{T}$ which were above the momentum values compared with ones which were initially below, at the high thrust (high collective angle) conditions. This correction to the formulation of the induced velocity function accounted for the difference in steady section angles-of-attack needed to bring the high collective pitch angle results into agreement with experiment.

Basic Considerations of Blade Kinematics

The high relative torsional stiffness of the "stiff" flexure, cases 3 and 5 of configuration IIA (see Figure 2), result in these cases taking on especially useful significance. For these two cases, the rotor blade is essentially rigid in torsion up to the point just outboard of the flexure. Thus, they are aeroelastically equivalent and should have the same stability characteristics. The experimental results shown in Figures 3c and 3e do confirm this supposition.

Within the context of the G400 technology, however, cases IIA-3 and IIA-5 must be respectively modeled as a blade with a straight elastic axis preconed at a 5 degree angle, and as a blade without precone, but with a 5 degree bend in the elastic axis. The effective equivalency of cases IIA-3 and IIA-5 thus forms the basis for validating the consistency of formulations especially with regard to elastic axis offset (structural sweep).

The aeroelastic significance of both radial foreshortening and spanwise tension (treated in the subsequent subsections) is that they are each an important source of coupling between flatwise bending and edgewise bending. Because of the contributions of flatwise bending to radial foreshortening, flatwise rate terms appear in the Coriolis force dependent terms in the edgewise equation. Similarly, because of the contribution of edgewise rate to the centrifugal force, edgewise rate terms appear in the tension terms in the flatwise equation. Because of the evident significance of these terms, a useful test for assessing the accuracy and self-consistency of the improved formulations was that the stability predictions for cases IIA-3 and IIA-5 be the same.

Kinematics of Radial Foreshortening

The original G400 development [1] invoked various principal assumptions which were intended to allow for advancement of the art of modeling nonlinear structural twist while avoiding unnecessary obfuscation caused by the inclusion of numerous nonlinear terms. Accordingly, the radial foreshortening of a mass element due to elastic bending, u_e, was kept simplistic and assumed to be limited to that accruing from flatwise bending only. It was accordingly represented by a quadratic function in flatwise bending:

$$u_e = \frac{1}{2} \sum_{i,m} \left[\int_0^r \gamma'_{w_i} \gamma'_{w_m} dr_l \right] q_{w_i} q_{w_m} \tag{7}$$

In the reformulated G400 technology[4], this restirctive assumption was relaxed. The two basic assumptions which were retained, expanded upon and utilized as an alternative basis are as follows:

1) The elastic (torsion axis is defined to be the spanwise locus of shear centers of the two-dimensional blade (beam) sections taken perpendicular to this spanwise locus. Note that this definition treats the elastic axis as an abstracted section property, as contrasted with what one would measure in a bench test of an actual curved beam. The built-in structural sweep (elastic axis offset), together with the elastic bending deflections, define an elastic axis which is generally a space-curve about which the local torsion deflection must take place.

2) The arc length of the so-defined elastic axis is invariant both in toto and per blade segment. Radial foreshortening accrue entirely from the kinematics of bending and distributed torsion along the space-curve elastic axis.

3) Local radial foreshortening is defined relative to the total extended arc length of the elastic axis. A hypothetical beam formed by the straightening out of the arc length of the elastic axis and the elimination of all pitch and twist is herein defined to be the "equivalent beam."

Contributions to radial foreshortening then accrue from (a) the built-in structural sweep, i.e. that which restores the equivalent beam to the original swept planform (b) first order (linear) functions of bending, arising from built-in structural sweep, (c) second order (nonlinear) functions of bending each with elastic torsion arising from built-in structural sweep, and (d) second order functions each of both flatwise and edgewise bending. These contributions are pictorially indicated in Figure 5.

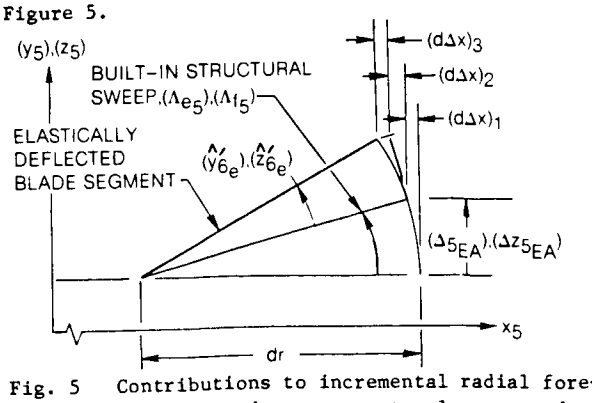

Fig. 5 Contributions to incremental radial foreshortening due to structural sweep and elastic deformations.

Each of these contributions can be modeled in a straightforward manner, and in lieu of the detailed development given in Reference 4, are simply stated as follows:

$$(d\Delta x)_1 = dr - dx = dr - \sqrt{dr^2 - \Delta y_{5_{EA}}^2 - \Delta z_{5_{EA}}^2} \tag{8}$$

$$= dr\left[1 - \sqrt{1 - (\Delta y_{10_{EA}}/\Delta r)^2 - (\Delta z_{10_{EA}}/\Delta r)^2}\right]$$

$$(d\Delta x)_2 = dr\left[\sin\Lambda_{f_5}\cos\Lambda_{e_5}\hat{z}'_{6_e} - \sin\Lambda_{e_5}\cos\Lambda_{f_5}\hat{y}'_{6_e}\right] \tag{9}$$

$$(d\Delta x)_3 = \cos\Lambda_{e_{5_0}}\cos\Lambda_{f_{5_0}}\left[1 - \sqrt{1 - v_e'^2 - w_e'^2}\right] dr$$

$$\cong \cos\Lambda_{e_{5_0}}\cos\Lambda_{f_{5_0}}\cdot\frac{1}{2}(v_e'^2 + w_e'^2)\,dr \tag{10}$$

where $\Delta y_{10_{EA}}$ and $\Delta z_{10_{EA}}$ are, respectively, the built-in changes per segment length of the chordwise and flatwise distances of the elastic axis from the reference, x_5, axis. And where Λ_{e_5} and Λ_{f_5} are, respectively, the structural sweep angle projections onto the x_5-y_5 and x_5-z_5 reference planes.

The total elastic radial foreshortening at the center of the nth segment is then determined by the following integral:

$$u_{e_n} = \int_0^{r_n}\left[(d\Delta x)_1 + (d\Delta x)_2 + (d\Delta x)_3\right] \tag{11}$$

The details of this integration are straightforward but sufficiently tedious to be beyond the intent and usefulness of this paper. Symbolically, u_e is finally given by:

$$u_e = (DUEAO) + (DUEAF_i)q_{w_i} + (DUEAE_k)\cdot q_{v_k}$$

$$+ (UELSET_{k_j})\,q_{v_k}q_{\theta_j} + (UELSFT_{i_j})\,q_{w_i}q_{\theta_j}$$

$$+ \frac{1}{2}(UELASE_{km})q_{v_k}q_{v_m} + \frac{1}{2}(UELASF_{in})\,q_{w_i}q_{w_n} \tag{12}$$

This formulation thus contains Equation 7 as a contributing term.

Spanwise Tension Distribution

Of all the terms appearing in the blade dynamic equations, the tension force is by far the greatest in magnitude and, by definition, qualifies as a "zeroth order" term. The difficulty in accurately modeling tension is that although it is a zeroth order term, the zeroth order component is equilibrated by other zeroth order effects (e.g. the steady blade airloads). Indeed, it can be well appreciated that the significant dynamics of rotor blades are determined by the higher order terms. Thus, even though tension is principally a zeroth order quantity, it still becomes important to model it with sufficient detail to capture the salient higher order effects.

Tension has been typically calculated as the direct spanwise integration of the radial force loading, S_{x_2}, outboard of the blade field point (center of blade segment). The radial force loading is, in turn, taken to be that due to centrifugal force and is thus dependent on the mass element radial position and inplane velocity, both of which include higher order terms. The formulations of the previous subsection, therefore, clearly impact on the calculation of centrifugal force. In addition to these reformulations, an additional higher order effect relating to tension was identified which subsequently led to the required self-consistency. In the reformulated G400 technology, account has been taken of the fact that tension is a vector whose local direction is determined by the orientation of the beam element (blade segment). The centrifugal force on the other hand is a vector always oriented radially in the rotor rotation plane. Hence, tension and centrifugal force are not generally codirectional. Upon defining the out-of-plane and inplane projections of the skew angle, γ, between these two vectors, as γ_F and γ_E, respectively, the effect of non-codirectionality on tension can be written as:

$$T(r) = F_T(r)\int_r^1 S_{x_2}\,dr_1 \tag{13}$$

where:

$$F_T(r) = \cos\gamma(r) = \sqrt{1 - \sin^2\gamma_E - \sin^2\gamma_F} \tag{14}$$

Reformulations Relating to Variable Elastic Axis Offset

As originally formulated, the G400 technology assumed the elastic axis to define a space-curve as a result of combined flatwise and edgewise bending. In this case, the blade curvature is directly proportional to the elastic modal degrees-of-freedom. This situation consequently allowed for considerable simplicity in structural modeling especially with regard to the nonlinear torsion excitation resulting from combined flatwise and edgewise bending (the ΔEI term). For the case of built-in variable elastic offset (structural sweep) the accurate definition of such sweep in terms of its curvature becomes impractical. Also, while an approximation to the blade kinematics resulting from "small sweep" could be obtained heuristically by considering the structural sweep to consist of "pre-bends" in the elastic axis, this procedure becomes suspect at moderate to large structural sweep. These issues become important in cases IIA-1 and IIA-2 wherein large bending deflections occur at the high collective angles, and in case IIA-6 where the effects of structural sweep are most pronounced. The following subsections address these two issues.

Torsion Excitation due to Compound Bending

As given in Reference 1, and as recognized elsewhere in the literature, the torsion differential equation is comprised of three basic parts. The first part consists of the usual elastic stiffening terms, and the second consists of combinations of distributed moment loadings. The third part is comprised of the wholly nonlinear torsion loadings accruing from distributed force loadings acting on moment arms provided by curvature in the elastic axis. As given in Reference 1, the torsion equation is given by:

$$\underbrace{\left[GJ\theta_e' + \Theta K_A^2 T + \tfrac{1}{2}EB_1(\Theta'^2 - \theta_B'^2)\Theta' - EB_2\theta_B' v_e''\right]'}_{\text{(I) elastic stiffening}} = \underbrace{\left[-q_{x_5} - y_5' q_{y_5} - z_5' q_{z_5}\right]'}_{\text{(II) moment loadings}}$$

$$+ \underbrace{\left\{y_5'' \int_r^1 \left[z_{5_1}' \int_{r_1}^1 p_{x_5}(r_2)\,dr_2 - \int_{r_1}^1 p_{z_5}(r_2)\,dr_2 + q_{y_5}(r_1)\right]dr_1 - z_5'' \int_r^1 \left[y_{5_1}' \int_{r_1}^1 p_{x_5}(r_2)\,dr_2 - \int_{r_1}^1 p_{y_5}(r_2)\,dr_2 - q_{z_5}(r_1)\right]dr_1\right\}}_{\text{(III) functions of force loadings}} \qquad (15)$$

curvatures

In Reference 1, the curvatures used in the (nonlinear) third portion of the torsion equation were assumed to arise entirely from the elastic bending deflections, v_e'' and w_e''. As such, it can be shown that the nonlinear excitation term in Equation (37) can be reduced to a compact expression which includes the familiar difference of bending stiffness term, ΔEI ($= EI_z - EI_y$):

$$\{\cdots\}_{(III)} = \left[(EI_z - EI_y)v_e'' w_e'' - (e_A T + EB_2(\theta_B' + \tfrac{1}{2}\theta_e')\theta_e')w_e''\right] \qquad (16)$$

This method for including the effect is attractive principally because of its simplicity and has been used to good advantage by numerous investigators. Three difficulties exist with this method of implementation, however. The first difficulty relates to the fact that the implementation of Equation (16) is based on a "mode deflection" description of internal bending moment. The difficulty with a mode deflection formulation per se is two-fold. Studies of the characteristics of mode deflection formulations (References 12 and 13) have established that convergence to accurate representations of internal bending moment is often not assured with a small number of modes. This accuracy problem is then compounded by the fact that the two components of this nonlinear excitation are subtractive. This is evidenced by the differencing of the section bending stiffnesses as indicated above.

A second difficulty with using the ΔEI method relates to the assumed space curve character of the elastic axis. As such, torsion deflections are seen to contribute to inplane and out-of-plane deflections in the presence of bending. Thus, an analogous nonlinear excitation exists in both the flatwise and edgewise bending equations. In the framework of the G400 technology, these nonlinear excitations in the bending equations are most practically implemented using a "force integration" approach. Consequently, the use of a ΔEI mode deflection implementation in the torsion equation together with a force integration implementation in the bending equations results in a (coupled) modal mass matrix which is generally nonsymmetric. A nonsymmetric mass matrix is not intrinsically a weakness for isolated rotor simulation and has been successfully used for years in that mode. However, the potential exists for spurious divergent response conditions caused by an inertia matrix becoming nonpositive-definite due to this deflection dependent nonsymmetry.

The third difficulty with the Equation 16 formulation is that it is difficult to include the built-in curvature due to structural sweep. Equation (16) requires curvature information which is not generally available for the built-in geometry.

Because of these difficulties, the conventional ΔEI approach of Equation (16) was abandoned in favor of a "force integration" approach. Accordingly, the Galerkin approach is first applied to the nonlinear excitation term and then integration by parts is used to achieve an intermediary step needed to eliminate the explicit curvature terms:

$$\int_0^1 \gamma_{\theta_j}\{\cdots\}_{(III)}\,dr = \int_0^1 \Big\{-p_{z_5}\int_0^{\bar r}\int_0^{\bar r_1}\gamma_{\theta_j} y_5''\,dr_2\,dr_1 + p_{y_5}\int_0^r\int_0^{r_1}\gamma_{\theta_j} z_5''\,dr_2\,dr_1 + (z_5' T + q_{y_5})\int_0^{\bar r}\gamma_{\theta_j} y_5''\,dr_1 - (y_5' T - q_{z_5})\int_0^{\bar r}\gamma_{\theta_j} z_5''\,dr_1\Big\}\,d\bar r \qquad (17)$$

Since this term represents the nonlinear effects, it is reasonable to use a zeroth order approximation to the curvature terms wherein the structural sweep is assumed to be "small". With this assumption, all the integrals in Equation (17) can be evaluated using the deflection correction functions defined in Reference 1.

Thus, Equation (17) becomes:

$$\int_0^l \gamma_{\theta_j} \{\cdots\}_{\textcircled{III}} dr = \int_0^l \{\Gamma_{y_{\theta_j}} [p_{y_5}\cos\Theta + p_{z_5}\sin\Theta] - \Gamma_{z_{\theta_j}} [p_{z_5}\cos\Theta - p_{y_5}\sin\Theta] + \tilde{\Gamma}_{z_{\theta_j}} [T(w_e' + z_{IO_{EA}}' - \Delta w^{(2)'} - \Delta w^{(2)'}) + q_{y_5}\cos\Theta + q_{z_5}\sin\Theta] - \tilde{\Gamma}_{y_{\theta_j}} [T(v_e' + y_{IO_{EA}}' + \Delta v^{(2)'} - \Delta v^{(2)'}) - q_{z_5}\cos\Theta + q_{y_5}\sin\Theta]\} dr \quad (18)$$

where:

$$\Gamma_{y_{\theta_j}} = \gamma_{\theta_j}(w_e + z_{IO_{EA}} - \Delta w - \Delta w) - (\Delta v_{EA_j} - \Delta v_{EA_j}) \quad (19a)$$

$$\Gamma_{z_{\theta_j}} = \gamma_{\theta_j}(v_e + y_{IO_{EA}} + \Delta v - \Delta v) - (\Delta w_{EA_j} + \Delta w_{EA_j}) \quad (19b)$$

$$\tilde{\Gamma}_{y_{\theta_j}} = \gamma_{\theta_j}(w_e' + z_{IO_{EA}}' - \Delta w^{(2)'} - \Delta w^{(2)'}) - (\Delta v_{EA_j}^{(2)'} - \Delta v_{EA_j}^{(2)'}) \quad (19c)$$

$$\tilde{\Gamma}_{z_{\theta_j}} = \gamma_{\theta_j}(v_e' + y_{IO_{EA}}' + \Delta v^{(2)'} - \Delta v^{(2)'}) - (\Delta w_{EA_j}^{(2)'} + \Delta w_{EA_j}^{(2)'}) \quad (19d)$$

Equation (18) represents the required form of the "force integration" implementation of the nonlinear torsion excitation term. Upon recognizing and utilizing various cancellations arising in Equation (18) itself and in combination with similar terms contained in the (II) moment loadings term, the final most useful form of the torsion equation can then be written as:

$$\int_0^l \gamma_{\theta_j}' [GJ\theta_e' + \cdots]' dr = \int_0^l \{\gamma_{\theta_j} q_{x_5} - \Gamma_{y_{\theta_j}} [p_{y_5}\cos\Theta + p_{z_5}\sin\Theta] + \Gamma_{z_{\theta_j}} [p_{z_5}\cos\Theta - p_{y_5}\sin\Theta] + (\Delta w_{EA_j}^{(2)'} + \Delta w_{EA_j}^{(2)'}) [T(w_e' + \cdots + q_{z_5}\sin\Theta] - (\Delta v_{EA_j}^{(2)'} - \Delta v_{EA_j}^{(2)'}) [T(v_e' + \cdots + q_{y_5}\cos\Theta]\} dr \quad (20)$$

To conclude this subsection, three observations can be made of the above formulations:

1. Equations (19) all reduce to zero for zero structural sweep and zero elastic deflection, as would be expected from the behaviour of Equation (16).

2. In Equation (18), the terms multiplying the nonlinear torsion weighting functions ($\Gamma_{y_{\theta_j}}$,...) are actually the force and moment loadings defined for the linear excitations of the bending equations. The nonlinear torsion weighting functions, Equations (19), thus serve in effect, as the virtual deflection functions arising from torsion deflections appropriate to the bending generalized loads.

3. The validity of the force integration approach is enhanced by the fact that the resulting terms in the torsion equation which represent rows of the inertia matrix (reflecting the integration of inertia forces) produce complete mass matrix symmetry and consequently insure positive-definiteness.

Kinematic Representation for Structural Sweep

The selected general approach to modeling structural sweep is to use the simple well established concepts for bending and torsion of straight beams as a departure point. Accordingly, blade elastic bending is defined by conventional beam bending differential equations wherein the usual independent spanwise variable is taken to be the arc length along the elastic axis. Furthermore, these bending differential equations are defined locally using the loadings normal to the built-in elastic axis. Within this context, explicit elastic bending-torsion coupling due to structural sweep is omitted in favor of implicit coupling due to inertial, aerodynamic and gravitational loadings taken with appropriate sweep related kinematics. Within this context, the major necessary task in modeling structural sweep is to define the kinematics of the blade element mass centers and aerodynamic centers as explicit functions of the blade modal response variables. This subsection addresses this major task, from which the formulations of inertial aerodynamic and gravity loads follow in a straightforward manner. These subsequent formulations for loadings are thus omitted herein for clarity.

Structural sweep is defined in a general sense wherein both inplane and out-of-plane offsets of the built-in elastic axis, $y_{5_{EA}}$ and $z_{5_{EA}}$, respectively, are admitted (see Figure 6). The basic objectives of the structural sweep related reformulations are: (1) to define a coordinate system rotation transformation from the "5" pitch axis system to the swept "6" system (which is locally attached to the elastic axis), and (2) to define the deflections in the "5" system as functions of the built-in structural sweep and the elastic bending and torsion motions, which are measured in the "6" system. These two objectives must also be met while including the previous G400 formulations with regard to structural twist. The procedure formulated for including these two structural elements (sweep and twist) is summarized in the material which follows; the reader is directed to Reference 4 for a more detailed description.

The general modeling of the blade y_5 and z_5 kinematics due to combined structural twist and sweep is accomplished in the following steps:

1. The elastic axis of the "equivalent beam" described in an above subsection is "distorted" back to the original planform defined by the built-in structural sweep and segment arc length distributions (but without pitch or twist). This step essentially defines the position in space of the elastic axis space curve. This positioning requires the x_5, y_5 and z_5 offset distances of the centers of the segments as well as projections onto the x_5-y_5 and x_5-z_5 planes of the swept elastic axis line segments. These projections define the sweep angle distributions, Λ_{e_5} and Λ_{f_5}.

2. As shown in Figure 6, the orientations of the elastic axis line segments define the local "6" coordinate system. x_6 is defined parallel to the axis of the elastic axis line segment; y_6 is defined parallel to the x_5-y_5 plane, (+) in leading edge direction; z_6 is orthogonal to x_6 and y_6, (+) in the normally positive thrusting motion. It should be stressed that the result of step 1 is to produce, in addition to the inplane and out-of-plane offsets (Δy_5 and Δz_5) of the elastic axis from the (reference) x_5 pitch axis, a radial foreshortening (x_5) due to the constancy of the total arc length of the elastic axis. This Δx_5 foreshortening is given by the negative of u_e, as developed in the previous section.

3. The blade segments of the blade configuration resulting from steps 1 and 2 are then pitched and twisted about their respective elastic axis line segments (x_6 axis) to restore the blade back to its original built-in, but elastically undeflected position. The pitch and twist angles for each segment are defined relative to the y_6 axis.

4. The blade is then elastically deflected in torsion ($\theta_e = \sum_j \gamma_{\theta_j} q_{\theta_j}$) about the built-in space curve elastic axis as defined by $y_{10_{EA}}$ and $z_{10_{EA}}$ to define a first set of "small" incremental y_5 and z_5 deflections.

5. The blade is then elastically deflected in flatwise and edgewise bending (w and v, respectively in the presence of the torsion deflection) to define a second set of small incremental deflections. This second set of incremental deflections is measured in the "6" coordinate system and is governed by the basic G400 deflection correction transformations defined in Reference 1.

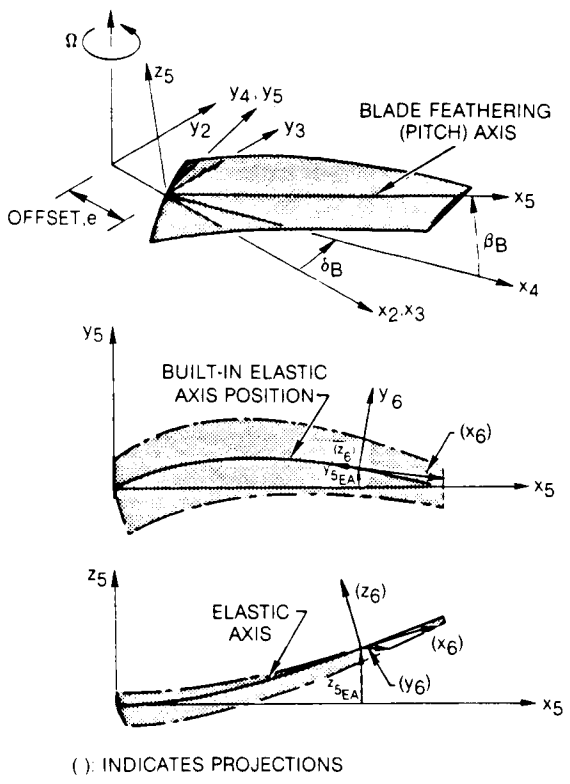

Fig. 6 Schematics of the "5" and "6" coordinate systems.

6. The second set of small incremental "6" coordinate system deflections defined in step 5 is transformed to the "5" coordinate system using an Euler angle transformation derived from sweep angle projections, Λ_{e_5} and Λ_{f_5}, as discussed in above step 1.

7. The results of steps 1, 4 and 6 are then combined to define the total y_5 and z_5 position vector components. These procedures are mathematically described by the following material.

First, the sweep angle projection distributions are defined using the built-in elastic axis line segment changes per segment length, the (invariant) segment arc lengths Δr, together with changes to the projection angles caused by elastic torsion deflection:

$$\Lambda_{e_5} = \sin^{-1}\left\{-\frac{\Delta y_{5_{EA}}}{\Delta r} - \left[\left(\Delta v_{EA_j}^{(2)'} - \Delta V_{EA_j}^{(2)'}\right)\cos\Theta + \left(\Delta w_{EA_j}^{(2)'} + \Delta W_{EA_j}^{(2)'}\right)\sin\Theta\right] q_{\theta_j}\right\} \quad (21)$$

$$\Lambda_{f_5} = \sin^{-1}\left\{\frac{\Delta z_{5_{EA}}}{\Delta r} + \left[-\left(\Delta w_{EA_j}^{(2)'} + \Delta W_{EA_j}^{(2)'}\right)\cos\Theta + \left(\Delta v_{EA_j}^{(2)'} - \Delta V_{EA_j}^{(2)'}\right)\sin\Theta\right] q_{\theta_j}\right\} \quad (22)$$

where $y_{5_{EA}}$ and $z_{5_{EA}}$ are the built-in elastic axis offset changes per segment length. For consistency with the definitions used for other previously defined radial distributions, these spanwise variable quantities are considered to be "derived" quantities calculated from the corresponding quantities defined in the chordwise and thicknesswise directions, $y_{10_{EA}}$ and $z_{10_{EA}}$, respectively. In practice, however, the "5" coordinate system quantities are the more accurately known and the "10" coordinate system quantities are derived using trigonometric resolution with the local built-in pitch angle.

The coordinate system transformation relating the pitch axis ("5") coordinate system with the swept ("6") coordinate system makes use of the sweep angle projections given in Equations (21) and (22):

$$\left\{\Delta X_6\right\} = \left[TAS\right]\left\{\Delta X_5\right\} \tag{23}$$

$$\left\{\Delta X_5\right\} = \left[TAS^{-1}\right]\left\{\Delta X_6\right\} = \left[TAS^{T}\right]\left\{\Delta X_6\right\} \tag{24}$$

where:

$$\left[TAS\right] = \begin{bmatrix} \chi & -\sin\Lambda_{e_5} & \sin\Lambda_{f_5} \\ \dfrac{\sin\Lambda_{e_5}}{\cos\Lambda_{f_5}} & \dfrac{\chi}{\cos\Lambda_{f_5}} & 0 \\ \dfrac{-\chi\sin\Lambda_{f_5}}{\cos\Lambda_{f_5}} & \dfrac{\sin\Lambda_{f_5}\sin\Lambda_{e_5}}{\cos\Lambda_{f_5}} & \cos\Lambda_{f_5} \end{bmatrix} \tag{25}$$

and where:

$$\chi = \sqrt{1 - \sin^2\Lambda_{e_5} - \sin^2\Lambda_{f_5}} \tag{26}$$

The above development can then be combined to yield the required expressions for inplane and out-of-plane displacement:

$$\begin{Bmatrix} y_5 \\ z_5 \end{Bmatrix} = \begin{Bmatrix} y_{10_{EA}}\cos\theta_B - z_{10_{EA}}\sin\theta_B \\ y_{10_{EA}}\sin\theta_B + z_{10_{EA}}\cos\theta_B \end{Bmatrix}$$

$$+ \sum_{j=1}^{NTM} \begin{Bmatrix} (\Delta v_{EA_j} - \Delta V_{EA_j})\cos\Theta + (\Delta w_{EA_j} + \Delta W_{EA_j})\sin\Theta \\ (\Delta v_{EA_j} - \Delta V_{EA_j})\sin\Theta - (\Delta w_{EA_j} + \Delta W_{EA_j})\cos\Theta \end{Bmatrix} q_{\theta_j}$$

$$+ \left[E\right]\left[TAS^{-1}\right] \begin{Bmatrix} 0 \\ (v_e + \Delta v - \Delta V)\cos\Theta - (w_e - \Delta w - \Delta W)\sin\Theta \\ (v_e + \Delta v - \Delta V)\sin\Theta + (w_e - \Delta w - \Delta W)\cos\Theta \end{Bmatrix} \tag{27}$$

where:

$$\left[E\right] = \begin{bmatrix} 0 & 1 & 0 \\ 0 & 0 & 1 \end{bmatrix} \tag{28}$$

and where v_e, w_e, Δv, Δw, ΔV, ΔW are linear and nonlinear combinations of q_{w_i}, q_{v_k}, and q_{θ_j}, as per the original G400 structural twist formulations (1). Thus, the objectives defined above have been met; the addition of structural sweep is accomplished while retaining the structural twist formulation. The formulation given by Equation (27) together with that for radial foreshortening, Equation (11), extends the kinematic modeling to applications with large structural sweep and moderate structural twist. Note that these formulations are generally quite nonlinear in the elastic modal response variables, q_{w_i}, q_{v_k} and q_{θ_j}.

Eigensolutions vs. Time-History Solutions

As shown in Figure 1, the basic G400 mathematical capability includes both an eigensolution and a time-history solution. Yet, despite the known advantages of eigensolutions, the time-history solution capability was used exclusively and produced results which were probably unattainable using the conventional eigensolution approach. The generally well-identified disadvantages of time-history solutions relative to eigensolutions (for stability calculations) are: (1) The calculation (CPU) time, and hence cost, is at least one order of magnitude greater; (2) the calculations inherently include the integral order forced responses which obscure assessment of the transients, and (3) postprocessing is required to obtain conventional stability descriptors.

The time-history solution, as formulated and implemented in the G400 technology, does not solve essentially linearized equations using an appropriate quadrature algorithm. Rather, the dynamic equations are retained in their nonlinear (implicit) form without recourse to the explicit expansion of loadings (as is typically required for eigensolutions). For the present study, this compact implementation presented clear advantages which outweighed the above identified disadvantages: (1) the accuracy of the basic physical modeling is separated from the issue of selected linearization scheme (mathematical modeling); (2) there is no need to calculate accurate equilibrium trimmed responses (as required for eigensolution linearization schemes), and, most significantly, (3) the compact implicit modeling scheme allows physical modeling modifications to be made easily to the coding and then quickly evaluated. It should be stressed that these advantages are related mostly to research and methodology development issues. For routine production calculations, the cost-effectiveness of eigensolutions is not to be denied. Thus, a synergistic relationship is implied between time-history solution and eigensolution development. The former is the superior physics modeling tool needed by the

latter before the mathematical modeling processes of linearization should occur. Clearly, the former provides an excellent alternate basis for validating the latter, whereas, the latter, once validated provides superior computational resources to the analyst.

Concluding Remarks

The challenge posed by the ITR/FRR Methodology Assessment study to correlate analyses with detailed experimental stability data has borne fruitful advances in the development of aeroelastic methodology. The United Technologies G400 analysis after being upgraded as a result of this study now appears to be well validated. Whereas, some of the reformulations constituting this upgrading are indigenous only to the G400 technology base, others appears to have general applicability to the field of rotor aeroelastics. These reformulations constitute, in part, some new solution techniques for some old problems: the inclusion of vortex-ring state effects into air mass dynamics, the kinematics of radial foreshortening, and a more accurate modeling of tension. More significantly, these reformulations constitute solution techniques for the relatively new problem area posed by combined variable structural sweep and structural twist. These latter reformulations should find useful application to a wide range of advanced rotor craft, such as aeroelastically conformable helicopter rotor blades, advanced technology propellers and prop-fans.

References

1. Bielawa, R. L., "Aeroelastic Analysis for Helicopter Rotor Blades with Time-Variable, Nonlinear Structural Twist and Multiple Structural Redundancy-Mathematical Derivation and Program User's Manual," NASA CR-2638, February 1976.

2. Bielawa, R. L., "A Second Order Nonlinear Theory of the Aeroelastic Properties of Helicopter Rotor Blades in Forward Flight," Ph.D. Thesis, Massachusetts Institute of Technology, June 1965.

3. Bielawa, R. L., "Aeroelastic Analysis for Helicopter Rotors with Blade Appended Vibration Absorbers - Mathematical Derivations and Program User's Manual," NASA CR-165896, June 1982.

4. Bielawa, R. L., Chi, R. M., Johnson, S. A., and Gangwani, S. T., "Aeroelastic Analysis for Propellers - Mathematical Formulations and Program User's Manual," NASA CR-3729, June 1983.

5. Bielawa, R. L., Cheney, M. C. Jr., Novak, R. C., "Investigation of a Bearingless Helicopter Rotor Concept Having a Composite Primary Structure," NASA CR-2637, October 1976.

6. Sopher, R., and Kottapalli, S.B.R., "Correlation of Predicted Vibrations and Test Data for a Wind Tunnel Helicopter Model," 38th Annual National Forum Proceedings, May 1982.

7. Anonymous, "Integrated Technology Rotor Methodology Assessment - Request for Proposal," NASA Ames Research Center, FRP 2-30221 (BR), September 1980.

8. Ormiston, R. A., and Bousman, W. G., "A Study of Stall-Induced Flap-Lag Instability of Hingeless Rotors," American Helicopter Society 29th Annual National Forum Proceedings, May 1973.

9. Peters, D. A., and Gaonkar, G. H., "Theoretical Flap-Lag Damping with Various Dynamic Inflow Models," Journal of the American Helicopter Society, Vol. 25, No. 3., July 1980.

10. Payne, P. R., Helicopter Dynamics and Aerodynamics, Pitman & Sons, Ltd., London, 1959.

11. Gessow, A., and Myers, G., Aeordynamics of the Helicopter, MacMillan Co., 1952, Republished by Frederick Ungar Publishing Company, New York, 1967.

12. Bisplinghoff, R. H., Ashley, H., and Halfman, R. L., Aeroelasticity, Addison-Wesley Publishing Co., Inc. 1957.

13. Bielawa, R. L., "Blade Stress Calculations Mode Deflection vs. Force Integration," Journal of the American Helicopter Society, Vol. 24, No. 3, July 1978.